Article

Cell Stem Cell

LIN28 Regulates Stem Cell Metabolism and Conversion to Primed Pluripotency

Graphical Abstract

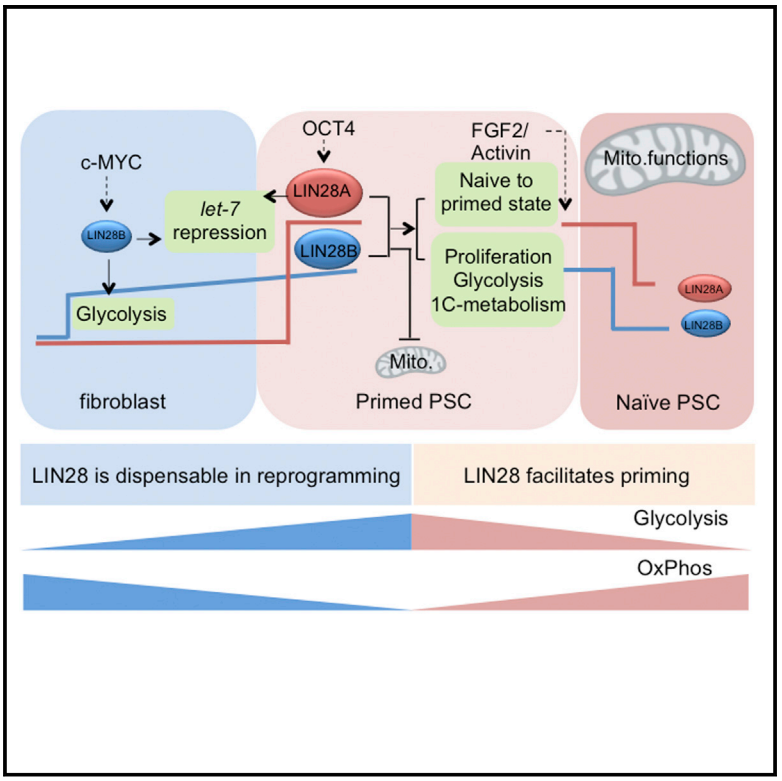

Authors

Jin Zhang,
Sutheera Ratanasirintrawoot,
Sriram Chandrasekaran, ..., Hu Li,
James J. Collins, George Q. Daley

Correspondence

george.daley@childrens.harvard.edu

In Brief

Zhang et al. show that the RNA binding protein LIN28A and its closely related paralog, LIN28B, play a key role in regulating pluripotent stem cell metabolism, including during reprogramming and pluripotency state transitions.

Highlights

- LIN28B functions equivalently to LIN28A in reprogramming to pluripotency
- In mouse, LIN28A and LIN28B facilitate transition from naive to primed pluripotency
- LIN28 regulates mouse iPSC metabolism by *let-7*-dependent and -independent mechanisms
- LIN28 binding to mRNAs regulates the metabolic proteome

Accession Numbers

GSE67568

Zhang et al., 2016, Cell Stem Cell *19*, 66–80
July 7, 2016
http://dx.doi.org/10.1016/j.stem.2016.05.009

CellPress

Cell Stem Cell
Article

LIN28 Regulates Stem Cell Metabolism and Conversion to Primed Pluripotency

Jin Zhang,[1,2,15] Sutheera Ratanasirintrawoot,[1,2,15,16] Sriram Chandrasekaran,[3,4,5] Zhaoting Wu,[1,2] Scott B. Ficarro,[2,6] Chunxiao Yu,[2,7] Christian A. Ross,[8] Davide Cacchiarelli,[4,9] Qing Xia,[1,2,10] Marc Seligson,[1,2] Gen Shinoda,[1,2] Wen Xie,[1,2] Patrick Cahan,[1,2] Longfei Wang,[2,7] Shyh-Chang Ng,[1,2] Supisara Tintara,[1,2] Cole Trapnell,[4,9] Tamer Onder,[1,2] Yuin-Han Loh,[1,2,11,12] Tarjei Mikkelsen,[4,9] Piotr Sliz,[2,7] Michael A. Teitell,[13] John M. Asara,[14] Jarrod A. Marto,[2,6] Hu Li,[8] James J. Collins,[3,4,5] and George Q. Daley[1,2,*]

[1]Stem Cell Transplantation Program, Division of Pediatric Hematology Oncology, Boston Children's Hospital, Boston, MA 02115, USA
[2]Department of Biological Chemistry and Molecular Pharmacology, Harvard Medical School, Boston, MA 02115, USA
[3]Institute for Medical Engineering and Science, Department of Biological Engineering, and Synthetic Biology Center, Massachusetts Institute of Technology, Cambridge, MA 02142, USA
[4]Broad Institute of MIT and Harvard, Cambridge, MA 02142, USA
[5]Wyss Institute for Biologically Inspired Engineering, Harvard University, Boston, MA 02115, USA
[6]Dana-Farber Cancer Institute, Harvard Medical School, Boston, MA 02115, USA
[7]Laboratory of Molecular Medicine, Boston Children's Hospital, Harvard Medical School, Boston, MA 02115, USA
[8]Center for Individualized Medicine and Department of Molecular Pharmacology and Experimental Therapeutics, Mayo Clinic, Rochester, MN 55905, USA
[9]Department of Stem Cell and Regenerative Biology, Harvard University, Cambridge, MA 02138, USA
[10]State Key Laboratory of Natural and Biomimetic Drugs, Department of Chemical Biology, School of Pharmaceutical Sciences, Peking University, Beijing 100191, China
[11]Epigenetics and Cell Fates Laboratory, A*STAR Institute of Molecular and Cell Biology, Singapore 138673, Singapore
[12]Department of Biological Sciences, National University of Singapore, Singapore 117543, Singapore
[13]Department of Pathology and Laboratory Medicine, Broad Stem Cell Research Center and Jonsson Comprehensive Cancer Center, University of California, Los Angeles, Los Angeles, CA 90095, USA
[14]Division of Signal Transduction, Beth Israel Deaconess Medical Center and Department of Medicine, Harvard Medical School, Boston, MA 02115, USA
[15]Co-first author
[16]Present address: Faculty of Medicine, Chulalongkorn University, Bangkok 10330, Thailand
*Correspondence: george.daley@childrens.harvard.edu
http://dx.doi.org/10.1016/j.stem.2016.05.009

SUMMARY

The RNA-binding proteins LIN28A and LIN28B play critical roles in embryonic development, tumorigenesis, and pluripotency, but their exact functions are poorly understood. Here, we show that, like LIN28A, LIN28B can function effectively with NANOG, OCT4, and SOX2 in reprogramming to pluripotency and that reactivation of both endogenous LIN28A and LIN28B loci are required for maximal reprogramming efficiency. In human fibroblasts, LIN28B is activated early during reprogramming, while LIN28A is activated later during the transition to bona fide induced pluripotent stem cells (iPSCs). In murine cells, LIN28A and LIN28B facilitate conversion from naive to primed pluripotency. Proteomic and metabolomic analysis highlighted roles for LIN28 in maintaining the low mitochondrial function associated with primed pluripotency and in regulating one-carbon metabolism, nucleotide metabolism, and histone methylation. LIN28 binds to mRNAs of proteins important for oxidative phosphorylation and modulates protein abundance. Thus, LIN28A and LIN28B play cooperative roles in regulating reprogramming, naive/primed pluripotency, and stem cell metabolism.

INTRODUCTION

Somatic cells can be reprogrammed to pluripotency by OCT4 and SOX2 together with KLF4 and c-MYC (OSKM) or NANOG and LIN28A (OSNA) (Park et al., 2008; Takahashi and Yamanaka, 2006; Takahashi et al., 2007; Yu et al., 2007). Among the original reprogramming factors, LIN28A is the only one that is not a transcription factor (Yu et al., 2007), and its role in reprogramming is still poorly understood. LIN28A and its paralog, LIN28B, are RNA binding proteins that are highly expressed during embryogenesis but silent in most adult tissues (Viswanathan and Daley, 2010). Both proteins bind and inhibit biogenesis of the *let-7* family of tumor suppressor microRNAs to affect cell proliferation (Viswanathan and Daley, 2010; Zhu et al., 2011) and also directly bind to numerous mRNAs, influencing their translation by mechanisms that remain incompletely understood (Cho et al., 2012; Madison et al., 2013). Including LIN28A in the reprogramming cocktail accelerates reprogramming efficiency in a proliferation-dependent manner (Hanna et al., 2009), but the exact mechanism, and whether LIN28B functions similarly in the context of stem cells and reprogramming, remain unknown. LIN28B has been studied in various types of human cancer (Madison et al.,

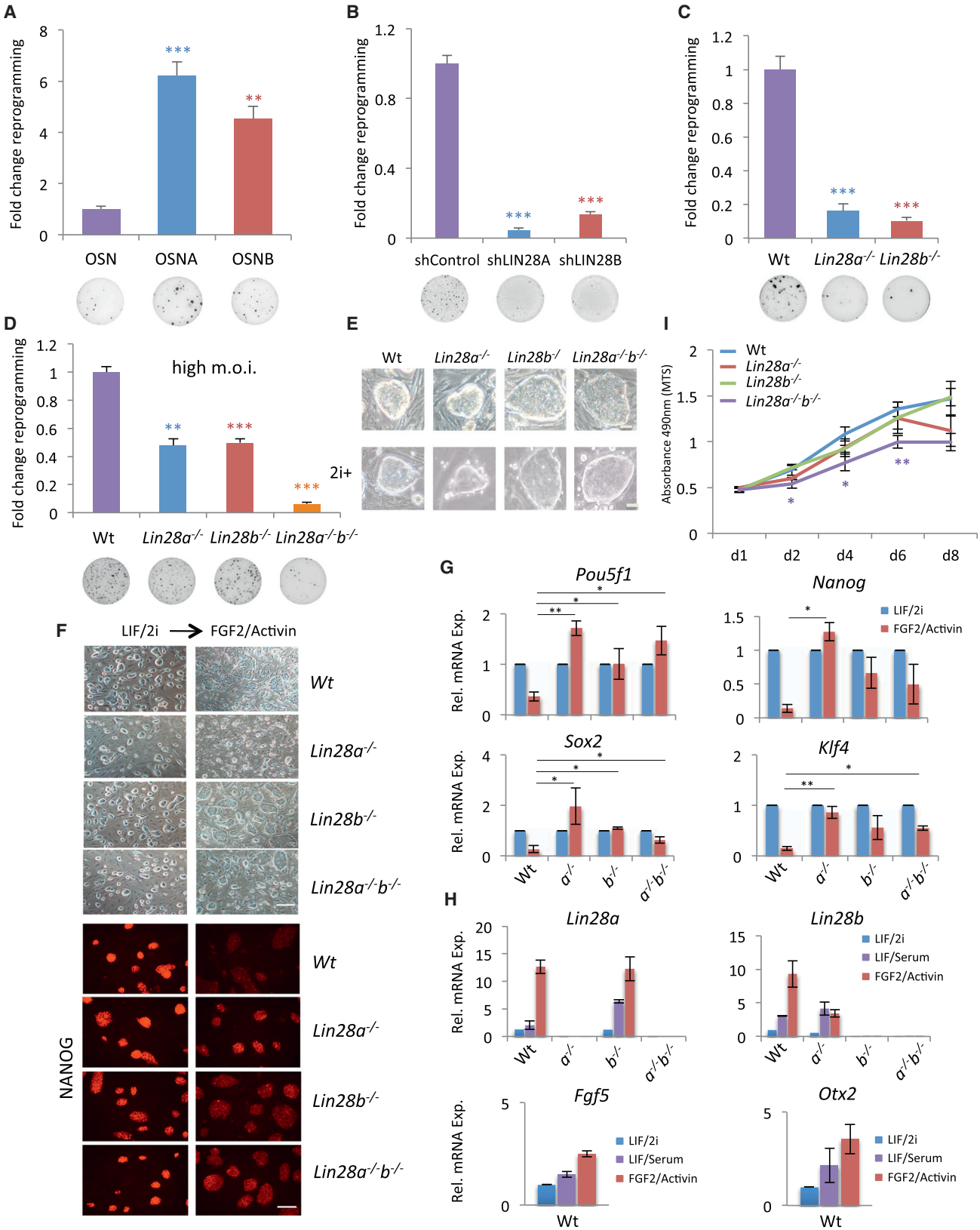

(legend on next page)

2013; Molenaar et al., 2012; Nguyen et al., 2014; Viswanathan et al., 2009) and, relative to LIN28A, has been reported to be differentially localized within cells and to function through distinct mechanisms (Piskounova et al., 2011), yet it has remained largely unexplored in the context of stem cells and reprogramming. It has been reported that *let-7* repression by an antisense inhibitor can promote reprogramming (Melton et al., 2010), but whether LIN28A and LIN28B regulate pluripotency entirely through *let-7*-dependent mechanisms, and whether the two paralogs play different roles, have not been explored.

Pluripotent stem cells (PSCs) have unique metabolic properties (Zhang et al., 2012). Somatic cell reprogramming resets cellular metabolism to a state of relatively high glycolysis and low oxidative phosphorylation (OxPhos) (Folmes et al., 2011), but the mechanism, particularly for repressed OxPhos, is still poorly understood. PSCs also rely on one-carbon metabolism for histone methylation and maintenance of pluripotency (Shiraki et al., 2014; Shyh-Chang et al., 2013a). In addition, both mouse and human PSCs are highly oxidative when in a "naive" state, in comparison to "primed" state cells (Huang et al., 2014; Takashima et al., 2014; Zhou et al., 2012), and *Lin28a* is expressed at markedly reduced levels in the naive versus primed states (Kumar et al., 2014; Marks et al., 2012). It is unknown what role LIN28 plays in conferring naive versus primed pluripotent cell fates and their associated metabolic status. While we previously reported that LIN28 regulates glucose metabolism through *let-7*-dependent mTOR signaling in the context of whole-animal physiology (Zhu et al., 2011), here, we reveal *let-7*- independent roles of LIN28 in regulating oxidative metabolism in mouse PSCs, including in *Dgcr8*$^{-/-}$ embryonic stem cells (ESCs), which lack microRNA (Wang et al., 2007), and roles of LIN28 in regulating one-carbon metabolism and PSC fate. Through functional analyses of metabolism, quantitative metabolomics and proteomics, and in vitro biochemistry, we demonstrate that LIN28A and LIN28B alter expression of metabolism genes that contribute to the unique metabotypes and cell states of pluripotency.

RESULTS

Both LIN28A and LIN28B Paralogs Contribute to Reprogramming

We first asked whether overexpression of LIN28B could function equivalently to LIN28A to promote efficient reprogramming of human somatic cells, and we found that both human LIN28A and LIN28B conferred ~4- to 6-fold increases in induced pluripotent stem cell (iPSC) colony formation when added to the OSN cocktail (Figure 1A). OSNB-derived iPSCs stained for SSEA-4 and TRA-1-60 expressed pluripotency genes and formed teratomas consisting of all three germ layers, indicating that they were bona fide fully reprogrammed PSCs (Figures S1A–S1C). To assess whether depletion of LIN28A or LIN28B similarly affected generation of OSKM-derived iPSCs, we infected dH1f human fibroblasts with small hairpin RNAs (shRNAs) against *LIN28A* or *LIN28B* prior to OSKM transduction and observed a significant reduction (>80%) of reprogramming efficiency for both paralogs (Figures 1B and S1D). To assess the LIN28 paralogs in murine reprogramming, we derived mouse embryonic fibroblasts (MEFs) from *Lin28a*$^{-/-}$, *Lin28b*$^{-/-}$, and *Lin28a*$^{-/-}$*b*$^{-/-}$ double-knockout embryos (Shinoda et al., 2013; Zhu et al., 2011), infected MEFs with the OSKM cocktail, and observed reductions in reprogramming efficiency for individual gene knockouts relative to wild-type MEFs (Figure 1C), with further reductions in the absence of both paralogs (Figure 1D). Taken together, these data suggest that LIN28B can promote reprogramming, comparably to LIN28A, when ectopically expressed but that both endogeneous genes are required for optimal reprogramming efficiency, implying complementary and incompletely redundant functions.

While mouse *Lin28a*$^{-/-}$ OSKM-derived iPSCs appeared morphologically similar to wild-type iPSCs, *Lin28b*$^{-/-}$ and *Lin28a*$^{-/-}$*b*$^{-/-}$ iPSC colonies appeared flatter (Figure 1E, top) but continued to stain for SSEA-1 and OCT4 by immunohistochemistry (Figure S1E). *Lin28a*$^{-/-}$*b*$^{-/-}$ iPSCs cultured in leukemia inhibitory factor (LIF)/serum media expressed most pluripotency marker genes at levels comparable to wild-type iPSCs, such as Oct4-*Pou5f1*, *Sall4*, and *Nr5a2*, but were lower for other marker genes, such as *Zfp42*, *Sox2*, *Tbx3*, *Nanog*, and *Gdf3* (Figure S1F). Interestingly, addition of the Mek/Erk pathway inhibitor PD0325901 and the GSK3β pathway inhibitor CHIR99021 (2i; Marks et al., 2012) to the LIF/serum media completely restored knockout iPSC morphology (Figure 1E, bottom) and expression of the pluripotent marker genes except for *Zfp42* (Figure S1G). Indeed, knockout cells cultured with 2i showed a modest increase of naive pluripotent markers *Klf4*, *Tbx3*, *Esrrb*, *Nr5a2*, and *Nanog* compared to wild-type cells (Figures S1G and S1H). Strikingly, they also resisted conversion to a primed state and maintained

Figure 1. Both LIN28A and LIN28B Paralogs Contribute to Reprogramming

(A) Fold change of reprogramming efficiency of human fibroblast dH1f transduced with OCT4, SOX2, and NANOG and cotransduced with empty vector (OSN), LIN28A (OSNA), or LIN28B (OSNB).

(B) Fold change of OCT4, SOX2, KLF4, and c-MYC (OSKM) reprogramming efficiency of dH1f infected with control, *LIN28A*, or *LIN28B* shRNA. Data represent three replicates of two independent shRNA hairpins against each gene. Representative TRA-1-60-stained reprogramming wells are shown for (A) and (B).

(C) Fold change of reprogramming efficiency 21 days after OSKM transduction of *Lin28a*$^{-/-}$ or *Lin28b*$^{-/-}$ MEFs relative to wild-type MEFs.

(D) Fold change of reprogramming efficiency at day 21 of wild-type and knockout MEFs infected with OSKM at high MOI (m.o.i.). Data represent two independent experiments with four replicates per cell line. Error bars represent SEM. *$p < 0.05$, **$p < 0.01$, and ***$p < 0.001$ (Student's t test). Representative SSEA-1-stained reprogramming wells are shown.

(E) Morphology of iPSCs derived from wild-type and knockout MEFs cultured in regular ESC media (top) and 2i+ media (bottom). Scale bar, 50 μm.

(F) Morphology and NANOG immunostaining of iPSCs converted from the naive condition (LIF/2i) to the primed condition (FGF2/activin) for 5 days. Scale bar, 500 μm.

(G) qRT-PCR showing pluripotent marker gene expression in iPSCs cultured in naive and primed states for 5 days. Data represent two independent experiments with four biological replicates. *$p < 0.05$, **$p < 0.005$ (Student's t test).

(H) qRT-PCR showing *Lin28a/b* and primed marker gene expression in iPSCs cultured in LIF/2i, LIF/serum, and FGF2/activin conditions.

(I) Proliferation rate measured by MTS cell proliferation assay. n = 3; *$p < 0.05$, **$p < 0.005$ (Student's t test).

See also Figure S1.

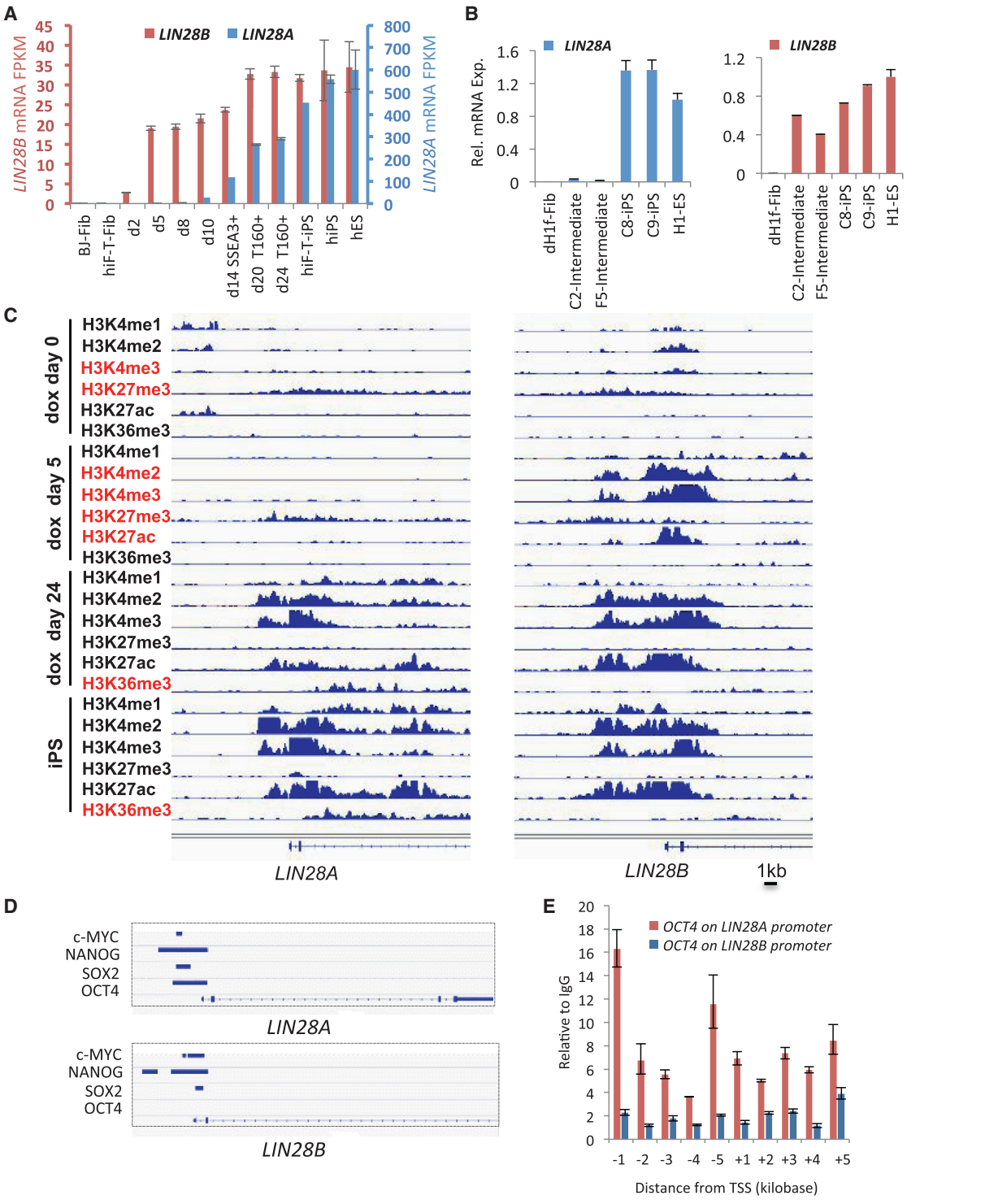

Figure 2. Differential Regulation of *LIN28A* and *LIN28B* in Reprogramming

(A) hTERT-immortalized human secondary fibroblasts (hiF-T-Fib) undergoing reprogramming were harvested at different days. BJ fibroblasts (BJ-Fib) and hiF-T-derived iPSCs (hiF-T-iPS) were included as controls. RNA-sequencing showed absolute mRNA level of *LIN28A* and *LIN28B*. Error bars show 95% confidence interval around the average values.

(B) qRT-PCR analysis of *LIN28A* and *LIN28B* mRNA level in partially reprogrammed cells (C2 and F5), fully reprogrammed iPSCs (C8 and C9), ESCs (H1), and fibroblasts (dH1f-Fib).

(legend continued on next page)

a dome-shape morphology and pluripotent gene expression after 5 days in primed media with fibroblast growth factor 2 (FGF2)/activin (Figures 1F, 1G, and S1I), suggesting *Lin28* promotes exit from the naive state of mouse PSCs. Overexpressing *let-7* also delayed priming, indicating *let-7*-dependency (Figure S1J). *Lin28a* and *Lin28b* also responded to FGF2 signaling, as they were upregulated upon switching from LIF/2i media to LIF/serum or FGF2/activin media, similar to other primed state marker genes *Otx2* and *Fgf5* (Marks et al., 2012) (Figure 1H). Despite defects in priming, *Lin28* knockout mouse iPSCs contributed to chimeras and formed teratomas with tissues from all three germ layers, demonstrating they are dispensable for maintaining pluripotency (Figures S1K and S1L). *Lin28* has been shown to confer a proliferative advantage during reprogramming (Hanna et al., 2009). While the difference in the proliferation rate in *Lin28a*$^{-/-}$ or *Lin28b*$^{-/-}$ iPSCs was not significant, *Lin28a*$^{-/-}$*b*$^{-/-}$ iPSCs proliferated more slowly than wild-type iPSCs (Figure 1I).

Differential Regulation of *LIN28A* and *LIN28B* in Reprogramming of Human Fibroblasts

To define the kinetics of endogenous *LIN28A* and *LIN28B* gene reactivation during OSKM-induced reprogramming, we examined mRNA levels of the hTERT-immortalized human fibroblast cell line hiF-T fibroblasts (Cacchiarelli et al., 2015) at different time points during reprogramming (Figure 2A). Interestingly, mRNA for endogenous *LIN28B* was detected as early as day 2 and was more than half maximal by day 4, while mRNA for endogenous *LIN28A* was not detected until days 8–10 and did not achieve maximal expression until late in reprogramming, implying differential gene reactivation. Isolation of the TRA-1-60+ population of cells late in reprogramming showed enriched expression of *LIN28A*, but not *LIN28B* (Figure S2A), implicating LIN28A as a stringent marker that is only upregulated upon acquisition of pluripotency, in contrast to LIN28B, which is a more promiscuous marker. We also examined the expression of the two paralogs in partially and fully OSKM-derived reprogrammed human cells (Chan et al., 2009) and found that *LIN28A* and a few other markers, such as *TDGF1*, *REX1*, *DAZL*, *DNMT3B*, *DPPA2/3*, and *ABCG2*, were exclusively expressed in fully reprogrammed iPSCs, whereas *LIN28B*, *NANOG*, *SALL4*, *GDF3*, *DPPA4*, and *DNMT3A* were expressed in both partially and fully reprogrammed cells (Figures 2B, S2B, and S2C). Interestingly, microarray analysis between partially and fully reprogrammed cells positioned *LIN28A* as the most differentially expressed gene (Figure S2D), together suggesting that late *LIN28A* expression marks bona fide iPSCs.

We next analyzed histone modifications associated with the *LIN28A* and *LIN28B* promoters at different time points during reprogramming in hiF-T fibroblasts (Figure 2C). At baseline, we detected H3K27me3 on the *LIN28A* promoter, consistent with its lack of expression in fibroblasts, while we detected both H3K4me3 and H3K27me3 on the *LIN28B* promoter, a bivalent mark associated with loci poised for expression. On day 5, H3K27me3 was still associated with the *LIN28A* locus, while the *LIN28B* locus was marked by H3K27ac, H3K4me2, and H3K4me3, all consistent with active *LIN28B* transcription. At day 24, *LIN28A* was expressed ten times higher than *LIN28B* (Figure 2A), and its gene body showed enhanced H3K36me3 that marks actively transcribed genes (Figure 2C). Consistent with the active chromatin state and expression of *LIN28A* in hiF-T-iPSCs (Figure 2C), analyses of existing genome-wide ChIP-sequencing data (Gifford et al., 2013) as well as ChIP-PCR showed that OCT4 has stronger binding at *LIN28A* promoter in PSCs (Figures 2D, 2E, and S2E). Together, these data suggest that for the human fibroblast cells we examined, the *LIN28B* locus assumes an active chromatin structure and reactivates gene expression earlier in reprogramming, while only later does *LIN28A* gain an open chromatin structure and gene activation and mark the bona fide reprogrammed cells.

Let-7-Independent Regulation of Oxidative Metabolism by LIN28 in Mouse PSCs

To further understand the molecular mechanisms by which LIN28A and LIN28B promote reprogramming, we performed microarray analysis with mouse wild-type and *Lin28*-deficient PSCs (Figure S3). Analysis of gene regulatory networks (GRNs) using the CellNet algorithm (Cahan et al., 2014) revealed that *Lin28a*$^{-/-}$*b*$^{-/-}$ iPSCs have a slightly altered ESC GRN (Figure S3B). Gene Ontology (GO) analysis indicated that the *Lin28b*$^{-/-}$ expression signature was enriched with metabolism-related GO terms such as "Mitochondrial inner membrane," "NADH dehydrogenase activity," and "Oxidative phosphorylation" and with amino acid-related metabolism terms such as "Glycine, serine and threonine metabolism," while the *Lin28a*$^{-/-}$ signature was enriched in "regulation of glucose metabolic process" (Figure S3D), suggesting that both paralogs influence cellular metabolism.

To dissect how LIN28A and LIN28B regulate metabolism, we measured cellular energetics of the mouse PSCs. The oxygen consumption rate (OCR)/extracellular acidification rate (ECAR) ratios for *Lin28b*$^{-/-}$ and *Lin28a*$^{-/-}$*b*$^{-/-}$ were increased relative to wild-type cells, resembling the more oxidative metabolic profile of MEFs (Figure 3A). Further analysis indicated that both *Lin28a*$^{-/-}$ and *Lin28b*$^{-/-}$ PSCs have elevated OCR (Figure S4A), while *Lin28a*$^{-/-}$ cells also have increased secretion of lactate, ECAR and LDHB protein (Figures S4A and S4C). These data indicate that both LIN28A and LIN28B repress OxPhos, while LIN28A might also repress glycolysis, in the context of mouse PSCs. The combined endogenous expression of LIN28A and LIN28B in wild-type cells corresponds with a more glycolytic and less oxidative metabolism reminiscent of the Warburg effect of cancer cells (Figure 3B), as reflected by their additive role in enhancing proliferation (Figure 1I). Elevated OCR in knockout cells is also consistent with more densely packed mitochondrial inner membrane cristae (Figure S4D). Overexpressing *Lin28b* in *Lin28a*$^{-/-}$*b*$^{-/-}$ iPSCs partially rescued the skewed metabolic phenotype (Figure 3C), consistent with the role of *Lin28b* in knockout cells.

(C) ChIP-sequencing was performed with hiF-T fibroblast cells with or without dox treatment and hiF-T-iPSCs. All plots are scaled to the value range 0–15.
(D) In silico analysis of ChIP-sequencing data of OCT4, SOX2, NANOG, and C-MYC in hESCs.
(E) ChIP-PCR using OCT4 antibody in hiPSCs. qPCR data were first normalized to input chromatin. n = 6; error bars represent SEM.
See also Figure S2.

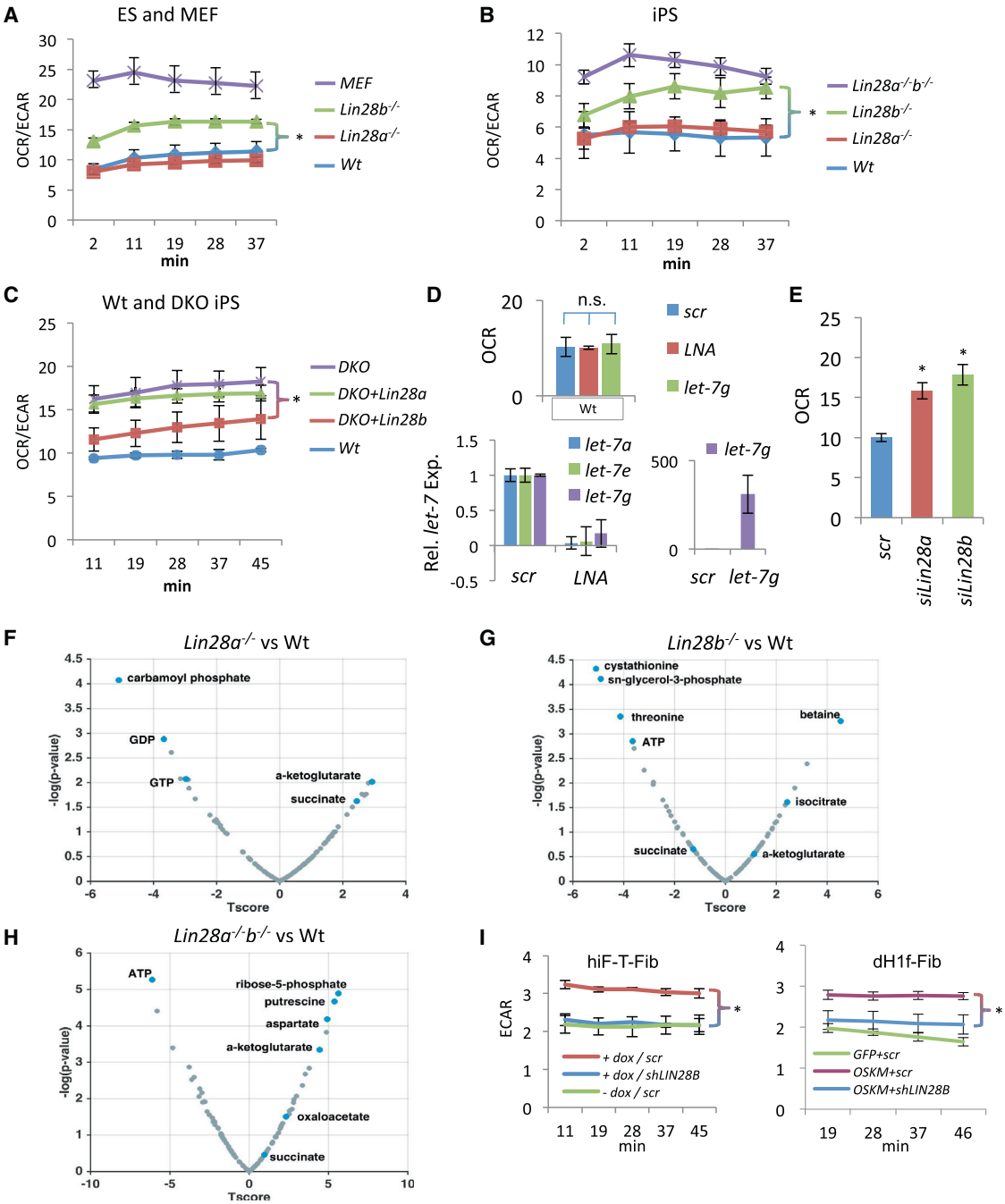

Figure 3. *Let-7*-Independent Regulation of Metabolism by LIN28

(A) OCR/ECAR for MEFs, wild-type ESCs, *Lin28*-deficient ESCs cultured in LIF/2i condition. n = 4; error bars represent SEM. *p < 0.05.

(B) OCR/ECAR for wild-type and *Lin28*-deficient iPSCs. n = 4; error bars represent SEM. *p < 0.05.

(C) OCR/ECAR for wild-type iPSCs and double-knockout iPSCs transfected with *Lin28a*- and *Lin28b*-overexpressing constructs and empty vector cultured in the LIF/2i condition. n = 3; error bars represent SEM. *p < 0.05.

(D) Top: OCR of wild-type ESCs transfected with *scramble (scr), LNA*, or *let-7g* mimic for 3 days. Bottom: *let-7* expression of the same cells. n = 4; n.s., not significant.

(E) OCR of *Dgcr8*$^{-/-}$ ESCs transfected with *scr*, *Lin28a*, or *Lin28b* siRNA for 3 days. n = 3; *p < 0.05.

(F–H) Volcano plots showing metabolomics analysis of *Lin28*-deficient versus wild-type iPSCs cultured in LIF/2i. T-score is the difference in mean between the samples divided by the SD. n = 12 for each phenotype.

(I) Left: ECAR of hiF-T fibroblasts treated with 2 μg/mL doxycycline and transduced with scramble or *shLIN28B* virus for 6 days. Right: ECAR of dH1f transduced with GFP or OSKM virus and scramble or *shLIN28B* virus for 3 days. n = 3; *p < 0.05. Error bars represent SEM.

See also Figures S3, S4, and S5 and Table S1.

To confirm the effects of LIN28A and LIN28B on PSC OxPhos, we also analyzed doxycycline-inducible *Lin28a/b*-overexpressing mouse ESCs (Zhu et al., 2011) and found that induction of *Lin28a/b* compromised basal and maximal OCR (Figures S4E and S4F), consistent with the loss-of-function lines (Figure S4B). Despite the hyper-induction of *Lin28* in ESCs, the levels of *let-7* did not change from their already suppressed levels (Figure S4G). In addition, either introducing a mature *let-7* mimic or inhibiting *let-7* with LNA (Figure 3D), or overexpressing *let-7* (Figure S4H) in wild-type cells did not change OCR, and transfection of a *let-7* mimic in *Lin28*-overexpressing cells did not reverse the reduced OCR (Figure S4I), suggesting that LIN28 reduced OCR through *let-7*-independent mechanisms.

To further exclude microRNA-dependent functions of LIN28A/B, we also assessed *Dgcr8*$^{-/-}$ mouse ESCs that are defective for microRNA biogenesis (Melton et al., 2010; Wang et al., 2007). Whereas knockdown of *Lin28a* resulted in upregulation of *let-7* in wild-type ESCs, knockdown in *Dgcr8*$^{-/-}$ ESCs did not affect the already scant quantities of *let*-7 (Figures S4J and S4K). Importantly, knockdown of either LIN28A or LIN28B in *Dgcr8*$^{-/-}$ ESCs resulted in a more oxidative phenotype, with 1.5- to 2-fold increase of OCR compared to control *Dgcr8*$^{-/-}$ ESCs (Figure 3E). Given the lack of microRNA function in *Dgcr8*$^{-/-}$ cells, these data demonstrate that LIN28A and LIN28B alter metabolism at least in part via *let-7*-independent mechanisms.

We previously reported that induction of LIN28A in transgenic mice promotes glucose tolerance and tissue repair (Shyh-Chang et al., 2013a; Zhu et al., 2011). Thus, we next asked whether LIN28A and LIN28B promote glucose metabolism in PSCs by tracing ^{13}C-glucose incorporation into metabolic pathway intermediate metabolites. Loss of LIN28A and LIN28B in mouse PSCs reduced ^{13}C labeling of glycolysis intermediates (Figure S5B). Acute *Lin28a/b* knockdown by small interfering RNA (siRNA) also led to slightly reduced ^{13}C labeling of the tricarboxylic acid (TCA) cycle intermediates in cells cultured in LIF/serum media (Figures S5C and S5D). Interestingly, switching culture conditions to LIF/2i naive media greatly increased glucose incorporation into the TCA cycle intermediates (Figure S5E), as recently reported (Carey et al., 2015), rescued the defects in glucose incorporation (Figure S5F), and enhanced the maintenance of knockout cells over multiple passages (Figure S5G). We also analyzed glutamine incorporation as well as steady-state metabolomics of cells cultured in LIF/2i media and found increased glutamine incorporation into the TCA cycle metabolites through oxidative metabolism (Figure S5H) and markedly increased absolute levels of TCA cycle metabolites in knockout cells, such as α-ketoglutarate, succinate, isocitrate, and oxaloacetate/aspartate (Figures 3F–3H), consistent with increased mitochondrial oxidative function. Interestingly, high α-ketoglutarate in ESCs is associated with naive pluripotency (Carey et al., 2015). We also found that supplemental α-ketoglutarate delayed naive to primed transition (Figure S5I), while reducing α-ketoglutarate by glutamine withdrawal accelerated the conversion (Figure S5J), presumably by increasing H3K9me3 (Carey et al., 2015) (Figure S5K). Altogether, the above functional and metabolomics data indicate that LIN28 represses mitochondrial oxidative metabolism in PSCs and plays a role in regulating the unique metabolic states of mouse naive and primed pluripotency.

We also analyzed LIN28 function in the early stage of reprogramming when endogenous *LIN28B*, but not *LIN28A*, is re-activated (Figure 2A). Knockdown of LIN28B decreased OSKM-induced glycolysis at day 3–6 of reprogramming in both hiF-T and dH1f human fibroblasts (Figures 3I and S5L), demonstrating that the boost in glycolysis observed early in reprogramming is at least partially attributable to *LIN28B* activation.

LIN28 Influences One-Carbon and Nucleotide Metabolism in Mouse PSCs

One-carbon metabolism encompasses the transfer of one unit of carbon from glucose, amino acids, or vitamins to support nucleotide biosynthesis, the maintenance of cellular redox state, and various methylation reactions (Locasale, 2013). In glucose-tracing experiments, we found that double-knockout cells have reduced glucose incorporation to serine (Figure 4A), which is a methyl group donor for one-carbon metabolism in nucleotide biosynthesis. Indeed, knockout cells were markedly depleted in nucleotides (Figures 3F–3H and 4B). In addition, extracellular metabolomics also showed that nucleosides and nucleotide bases were among the most downregulated metabolites in double-knockout cells (Figure 4C), suggesting nucleotides are either produced less or salvaged more in these cells. Supplementing cell culture media with a pool of nucleotide bases, but not purines or pyrimidines alone, rescued proliferation defects (Figures 4D and 4E), demonstrating that LIN28 supports nucleotide metabolism to enable PSC proliferation.

LIN28 Regulates Histone Methylation in Mouse PSCs

One-carbon metabolism also provides the methyl group to S-adenosyl-methionine (SAM), the donor of histone methylation (Figure 5A). We examined LIN28 knockout iPSCs and found lower ^{13}C incorporation from serine to SAM (Figure 5B) and hypomethylation of H3K9 and H3K27 (Figure 5C). Acute knockdown with siRNAs against LIN28A, but not LIN28B, showed hypomethylation (Figure 5D), consistent with the predominant expression of LIN28A in PSCs (Figure 2A). ChIP-PCR revealed lower levels of H3K9me3 and H3K27me3 at the promoters of *Nanog*, *Tbx3*, and *Pou5f1* (Figure 5E). Expression levels of these genes were higher in the knockout cells (Figures S1G and S1H), consistent with the findings that these cells have delayed exit from naive pluripotency (Figure 1F and 1G), which is associated with H3K9 hypomethylation (Marks et al., 2012). Supplementing SAM, but not homocysteine, rescued hypomethylation (Figure 5F), indicating SAM deficiency accounts for knockout cell hypomethylation. Supplementing the pool of nucleotide bases also partially rescued (Figure 5G), suggesting nucleotide deficiency in knockout cells can also influence histone methylation (Maddocks et al., 2016). Together, it appears LIN28 modulates histone methylation by enhancing one-carbon metabolism for methylation and repressing α-ketoglutarate and demethylation (Figure 5H).

LIN28 Regulates the Metabolic Proteome in Mouse PSCs

LIN28A and LIN28B proteins bind numerous mRNA molecules (Cho et al., 2012; Madison et al., 2013; Wilbert et al., 2012), and LIN28A has been reported to repress the translation of ER-associated transcripts (Cho et al., 2012). To examine the effects of

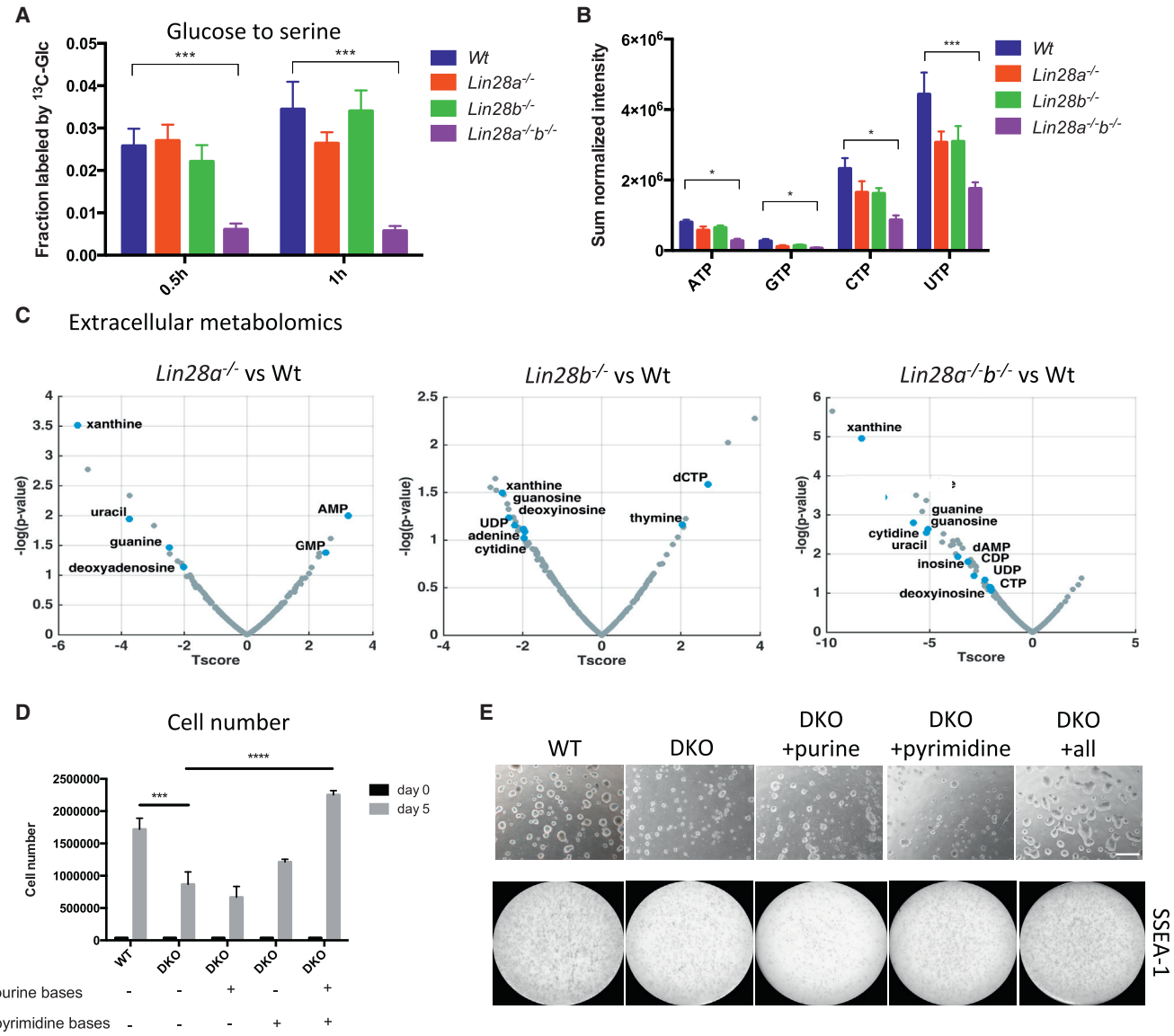

Figure 4. LIN28 Regulates One-Carbon Metabolism and Nucleotide Metabolism

(A) Fraction of serine labeled by [U^{13}C]-glucose in wild-type and *Lin28* knockout PSCs at 0.5 and 1 hr labeling times.

(B) Sum normalized total metabolite level in wild-type and knockout PSCs. For (A) and (B), n = 3; *p < 0.05, ***p < 0.001. Error bars represent SEM.

(C) Volcano plots showing extracellular metabolomics analysis of *Lin28*-deficient versus wild-type iPSCs. T-score is the difference in mean between the samples divided by the SD. n = 12.

(D and E) Number and morphology of wild-type and double-knockout (DKO) cells with and without supplementing nucleotide bases in the media for 5 days. Purine bases include adenine, guanine, inosine, and xanthine; pyrimidine bases include cytosine, uracil, and thymine. Each nucleobase has a concentration of 250 μM. Scale bar, 500 μm.

See also Table S2.

LIN28A/B on protein expression in mouse wild-type and *Lin28*-deficient ESCs, we performed stable isotope labeling by amino acids in cell culture (SILAC) followed by mass spectrometry (Figure S6A). Loss of LIN28A had a strong effect on the proteome, reflected by an increase in expression for ~16% of all quantified proteins, while LIN28B exhibited less impact on protein expression (Figure 6A and S6B), consistent with the 10-fold higher expression of *LIN28A* than *LIN28B* in ESCs (Figure 2A). Although our proteomic data encompassed some 30% of *let-7* targets, less than 1% of predicted *let-7*-regulated proteins were affected by LIN28 depletion (Figure 6B), suggesting that LIN28 influences protein abundance mainly through a *let-7*-independent mechanism in PSCs, which express low levels of *let-7*. GO categories of proteins whose levels were elevated in *Lin28b*$^{-/-}$ cells included "NADH dehydrogenase activity," "respiration chain," and "mitochondrion inner membrane," while proteins altered in *Lin28a*$^{-/-}$ cells were enriched in "mitochondrion" (Figure S6C). Gene set enrichment analysis (GSEA) also showed that the gene set associated

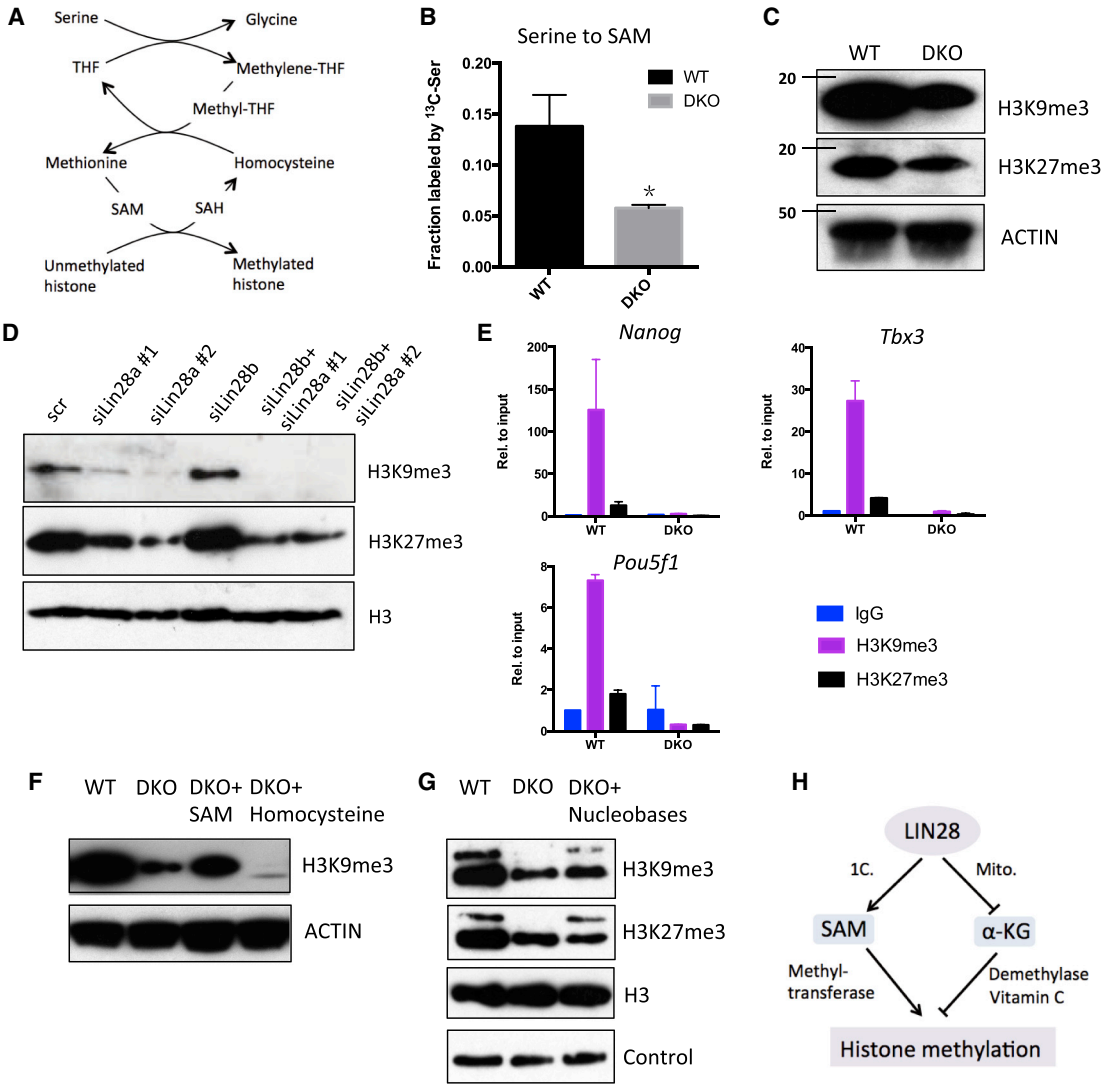

Figure 5. LIN28 Regulates Histone Methylation

(A) Serine provides a methyl group for histone methylation.

(B) Fraction of S-adenosyl-methionine labeled by [$U^{13}C$]-serine in wild-type and *Lin28* knockout iPSCs at 8 hr; n = 3. *p < 0.05.

(C) Western blotting showing H3K9me3 and H3K27me3 in wild-type and *Lin28* double-knockout (DKO) iPSCs.

(D) Western blotting showing H3K9me3 and H3K27me3 in wild-type iPSCs transduced with scramble, *Lin28a* or *Lin28b* siRNA for 5 days.

(E) ChIP-PCR with immunoglobulin G, H3K9me3, or H3K27me3 at promoters of indicated genes.

(F) Western blotting showing H3K9me3 in wild-type, DKO, and DKO cells supplemented with 1 mM SAM iodide or 1 mM homocysteine for 48 hr.

(G) Western blotting showing H3K9 and H3K27 tri-methylation in wild-type, DKO, and DKO cells supplemented with the same pool of all seven nucleobases as in Figure 4D.

(H) A schematic showing LIN28 regulates histone methylation.

with OxPhos was predominantly elevated in *Lin28b*$^{-/-}$ and, to a lesser extent, in *Lin28a*$^{-/-}$ ESCs (Figure 6C, top), as well as in LIN28B knockdown HEK cells compared to LIN28B-overexpressing HEK cells (Figure 6D) (Hafner et al., 2013). Western blotting confirmed that *Lin28a*$^{-/-}$ and *Lin28b*$^{-/-}$ ESCs have elevated expression of proteins involved in mitochondrial OxPhos complexes, including NDUFS3, NDUFB8, NDUFB10, SDHB, UQCRFS1, UQCRC2, and MTCO1, validating the proteomics results (Figure 6E). Further analysis also showed that proteins under-expressed in *Lin28a*$^{-/-}$ include "RNA splicing," as reported before (Wilbert et al., 2012), as well as "one-carbon metabolism" (Figures S6C and S6D). To examine the additive effect of loss of both loci, we analyzed *Lin28a*$^{-/-}$*b*$^{-/-}$ ESCs and iPSCs and found that "mitochondrion" and "oxidative phosphorylation" were the most enriched categories of proteins highly expressed in *Lin28a*$^{-/-}$*b*$^{-/-}$ ESCs and iPSCs (Figures 6C, 6F, and S6E). The double knockout also had reduced "glycolysis proteins" (Figures 6F and S6E), consistent with their lower glycolytic flux (Figure S4M), and reduced one-carbon metabolism and nucleotide metabolism proteins (Figures S6F and S6G). Western blotting

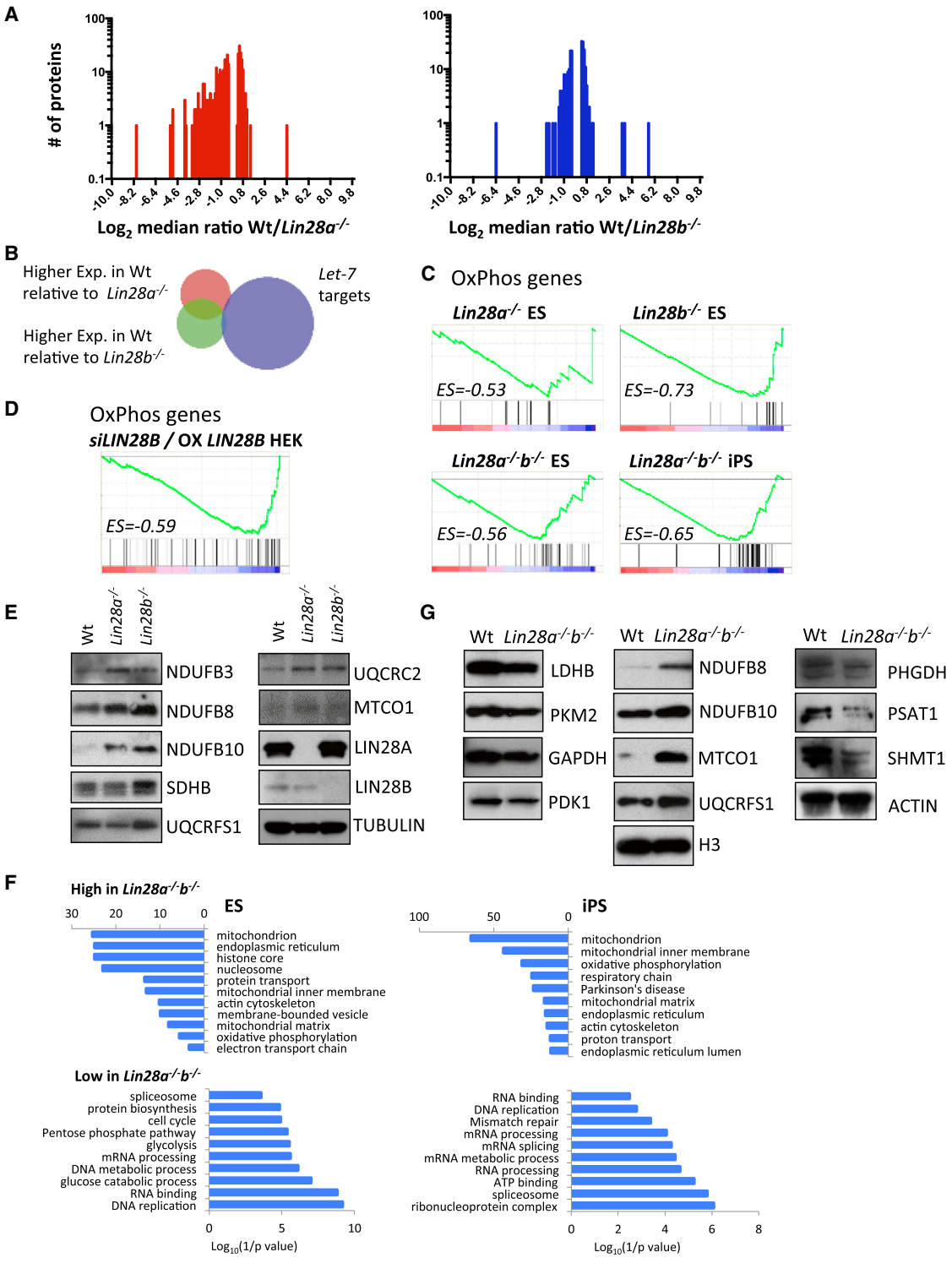

Figure 6. LIN28A and LIN28B Regulate the Metabolic Proteome

(A) Shown are the $\log_2$ median ratios of protein level between wild-type and knockout ESCs after 15-day labeling with SILAC media.

(B) Venn diagram showing overlap among *let-7* targets (from GSEA) and proteins that were decreased upon *Lin28a* or *Lin28b* knockout.

(C) GSEA analysis showing OxPhos proteins in the knockout ESCs and iPSCs (ES, enrichment score).

(D) GSEA analysis showing OxPhos proteins in the *siLIN28B* HEK cells compared to *LIN28B*-overexpressing HEK cells.

(E) Western blotting showing proteins changed in *Lin28a* and *Lin28b* knockout ESCs compared to wild-type cells.

(legend continued on next page)

analysis confirmed lower protein levels of LDHB, PKM2, GAPDH, PDK1 and PHGDH, PSAT1, and SHMT1 in double-knockout cells, whereas NDUFB8, NDUFB10, SDHB, UQCRFS1, and MTCO1 were expressed at higher levels (Figure 6G).

To understand whether LIN28A and LIN28B could directly bind mRNAs of metabolic proteins, we first performed in silico GO term analysis of published cross-linking immunoprecipitation sequencing (CLIP-seq) targets in ESCs and LIN28A-overexpressing HEK cells (Wilbert et al., 2012) and found that targets were enriched with "OxPhos," in addition to the reported "Spliceosome" (Figure S7A). We did not find enriched GO terms for glycolysis or one-carbon metabolism. We performed RNA immunoprecipitation PCR with LIN28A or LIN28B antibodies in human iPSCs and fibroblast cells. In iPSCs, both LIN28A and LIN28B bound the precursor of *let-7* microRNA, *OCT4* mRNA, and mRNA of the OxPhos genes (Figure S7B).

We further examined *Ndufb10* from OxPhos complex I because it appeared in five previous LIN28 RNA pull-down analyses as a common binding target (Figure S7C) (Cho et al., 2012; Hafner et al., 2013; Li et al., 2012; Peng et al., 2011; Wilbert et al., 2012). Using an electrophoretic mobility shift assay (EMSA), we found that LIN28 protein bound the *Ndufb10* 3′ end 30-bp RNA oligo containing a putative GGAG binding site (Nam et al., 2011; Wilbert et al., 2012), as well as *pre-let-7g*, but not a poly-AUCG-negative control (Figures 7A and 7B). We detected no binding to a 30-bp RNA oligo from the 5′ end, consistent with CLIP-seq data (Figures 7A and 7C), and binding to the 3′ RNA oligo was impaired for the *Ndufb10* ΔGGAG or GGAU mutants or when LIN28 cold shock domain alone was tested, suggesting that binding is dependent on recognition of the *GGAG* motif of the mRNA by the LIN28 zinc knuckle domains (Figures 7D and 7E). Interestingly, *Ndufb10* mRNA half-life was extended (Figure S7D) and its protein abundance was increased in *Lin28*-depleted mouse iPSCs (Figure S7E), demonstrating *Ndufb10* is a functional target of LIN28. *let-7* expression was not changed in *Lin28b*$^{-/-}$ cells, indicating that changes in mRNA half-life and protein abundance were *let-7* independent (Figures S7F). Other OxPhos mRNAs such as *Ndufb3, Ndufb8*, and *Uqcrfs1* also showed strong binding (Figures 7F, S7G, and S7H), and their protein level was also repressed by LIN28 (Figures 6E and 6G). Using biotinylated *Ndufb3* and *Ndufb10* RNA oligos with the same sequence as that used for EMSA, we were able to pull down more LIN28 protein using wild-type oligos compared with GGAG mutants (Figure S7I). Functionally, the mRNA half-lives of the OxPhos gene set (enriched in LIN28 binding targets) tended to be increased in knockout cells (Figure S7J). Together, these data demonstrate that LIN28 binds mRNA and regulates expression of genes critical for mitochondrial OxPhos function.

DISCUSSION

In summary, we have demonstrated that when overexpressed, LIN28A and LIN28B can both enhance iPSC derivation efficiency, while loss of endogenous LIN28A/B reduces reprogramming efficiency and traps the derived mouse iPSCs in a more naive state. Both paralogs bind to mRNAs for OxPhos genes, repressing their protein abundance and conferring the low mitochondrial metabolism characteristic of primed state pluripotency (Folmes et al., 2011; Zhou et al., 2012), which has higher LIN28 expression compared with the naive state. LIN28A influences the abundance of a broader range of proteins, while LIN28B primarily confers the embryonic type of low-OxPhos high-glycolysis metabolism, and its locus is bound and regulated by c-MYC (Chang et al., 2009), which also potentiates glycolysis in the early stages of reprogramming (Folmes et al., 2013). Considering the co-expression of both paralogs in embryonic tissue and high-frequency LIN28B expression in multiple types of cancer (Piskounova et al., 2011; Viswanathan and Daley, 2010), their upstream regulation and downstream functions revealed in PSCs here are likely to shed light on both early embryonic development and cancer.

Despite being a well-known pluripotency factor, *Lin28* is reduced in the LIF/2i ground state (Kumar et al., 2014; Marks et al., 2012) and highly expressed in the primed state of pluripotency in mouse PSCs. We have shown that *Lin28* is not only a marker associated with primed pluripotency but also facilitates the mouse naïve-to-primed state transition induced by FGF/activin signaling. Although our finding applies to the mouse naive state, we believe a similar mechanism pertains to human cells, given the lower LIN28A and LIN28B expression in human blastocysts compared with cultured, primed hESCs (Yan et al., 2013). This finding is also reminiscent of previous studies in other model systems. *Lin28* is required for development of *Xenopus* embryos in response to FGF and activin/nodal-like mesoderm-inducing signals involved in germ layer specification (Faas et al., 2013).

One emerging feature of naive pluripotency is its unique metabolism, including elevated mitochondrial function (Huang et al., 2014; Takashima et al., 2014; Zhou et al., 2012), increased glucose oxidative metabolism via the TCA cycle (Carey et al., 2015), and lower levels of SAM required for methylation (Sperber et al., 2015). One of the main metabolic contributions of mitochondrial oxidative metabolism in proliferating cells is to provide NAD^+ as an electron acceptor with oxidizing potential, which facilitates aspartate production through the TCA cycle (Birsoy et al., 2015; Sullivan et al., 2015). Other TCA cycle metabolites such as a-ketoglutarate are also linked to respiration (Sullivan et al., 2015). In mouse PSCs, we show that a-ketoglutarate and aspartate are among the most upregulated metabolites in *Lin28* knockout cells, and this upregulation is accompanied by increased glutamine oxidative metabolism. Availability of extracellular glutamine and intracellular a-ketoglutarate appears to impact histone marks such as H3K9me3 and H3K27me3, due to the role of a-ketoglutarate as a cofactor of histone demethylase (Carey et al., 2015). Accordingly, increased respiration and altered homeostasis of a-ketoglutarate in *Lin28* knockout cells can also influence chromatin states and promote activation of naive marker genes. On the other hand, LIN28 modulates the one-carbon metabolism pathway to directly impact the donor

(F) Shown are the top GO terms enriched in proteins changed in *Lin28a*$^{-/-}$*b*$^{-/-}$ ESCs or iPSCs compared with wild-type cells after 15-day labeling with SILAC media.

(G) Western blotting showing proteins changed in *Lin28a/b* double-knockout ESCs compared to wild-type cells.

See also Figure S6.

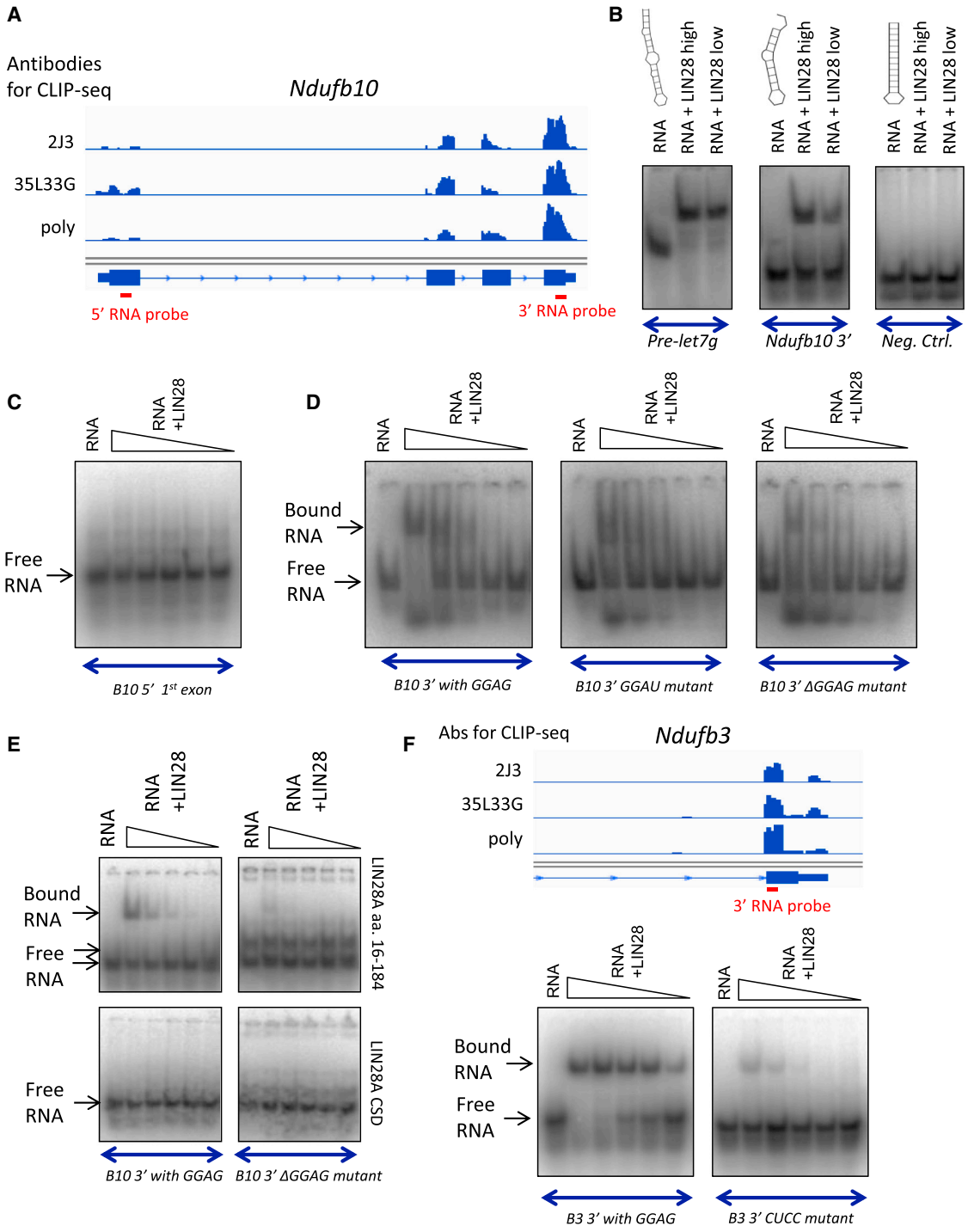

Figure 7. LIN28 Specifically Binds OxPhos Gene mRNAs

(A) CLIP-seq showing LIN28A binding peaks at *Ndufb10* mRNA. Red bars indicate the positions of the RNA oligo probes used in the following EMSA assays.

(B) EMSA showing mouse LIN28 (aa 16–184 containing conserved RNA binding cold shock and zinc knuckle domains) binding to *pre-let-7* and *Ndufb10* 3′ end synthesized RNA oligos; negative control is a poly-AUCG RNA oligo probe.

(C) EMSA showing the absence of LIN28 binding to the 5′ first exon RNA oligo. *B10: Ndufb10*.

(D) EMSA showing reduced LIN28 binding at mutant *Ndufb10* 3′ RNA oligo. *GGAG* → *GGAU* point mutation; *ΔGGAG* → *GGAG* deleted. Triangle block indicates a gradient concentration of LIN28 recombinant protein, from left to right: 12.5 μM, 6.25 μM, 2.08 μM, 0.69 μM, and 0.23 μM.

(legend continued on next page)

of histone methylation, SAM, and to influence histone modification and gene expression. This regulation seems to be dependent on *let-7* as overexpression of LIN28 and *let-7* reciprocally influence PSC one-carbon pathway metabolite abundance (Shyh-Chang et al., 2013a). Also, LIN28 regulation of the one-carbon pathway influences nucleotide metabolism and confers more proliferative capacity on primed cells.

To our surprise, the effect of LIN28 on oxidative metabolism appears at least in part to be *let-7* independent, given that knockdown of LIN28 in a microRNA-free system also changed respiration, while manipulating *let-7* level in wild-type cells did not. The LIN28 effects appear to be context dependent, based on the availability of its many RNA targets. During the early stages of reprogramming, when there is abundant *let-7* precursor transcription, LIN28 is bound and likely saturated by this class of abundant high-affinity targets, and thus it promotes reprogramming mainly by repressing *let-7* biogenesis. In established iPSCs with less *let-7* transcription, LIN28 is free to interact with its other RNA targets and regulate their functions, including those OxPhos mRNAs that harbor LIN28 binding sites.

The exact mechanism by which LIN28 regulates its mRNA target function may involve multiple levels of mRNA metabolism. LIN28 could potentially bind precursors of mRNAs and regulate alternative splicing and alternative polyadenylation (Wilbert et al., 2012); alternatively, LIN28 could recruit RNA helicase to change the secondary structure of mRNA and influence translation (Cho et al., 2012; Jin et al., 2011), or LIN28 binding could recruit TUTase to uridylate the mRNA 3′ end to mediate mRNA degradation (Heo et al., 2009; Lim et al., 2014). We determined that the half-lives of OxPhos mRNAs were globally increased in the knockout cells, demonstrating a probable role for LIN28 in regulating the mRNA stability of a specific set of genes. We also noticed that the regulation of OxPhos gene expression in PSCs is different from previously reported in MEF cells (Shyh-Chang et al., 2013b) and is likely due to the highly distinct contexts of these two different cell types. We have not found enrichment of glycolysis or one-carbon metabolism mRNAs as LIN28 targets, suggesting their regulation by LIN28 might be through other mechanisms, such as indirectly through *let-7* (Shyh-Chang et al., 2013a; Zhu et al., 2011). Thus, it will be of great interest to further investigate different mechanisms of how LIN28 regulates its downstream effectors in various contexts.

EXPERIMENTAL PROCEDURES

Cell Culture

Fibroblasts were cultured in DMEM (11960-069) containing 10% FBS (06902, STEMCELL Technologies) and 1% sodium pyruvate (11360-070, Invitrogen). Mouse iPSCs and ESCs were cultured in mouse ESC media (LIF/serum) comprising knockout DMEM (10829-018, Gibco) containing 15% FBS, 100 μM MEM-NEAA (11140-050, Invitrogen), and 1000 u/ml mLIF (ESG1107, Millipore) with 50 μM 2-mercaptoethanol (M7522-100ML, Sigma). Human iPSCs and ESCs were cultured in hESC media comprising DMEM/F12 (11330-057, Invitrogen) containing 20% KOSR (10828-028, Invitrogen), 100 μM MEM-NEAA, and hFGF2 (PHG0266, Invitrogen) with 50 μM 2-ME. Media is supplemented with 200 μg/mL penicillin, 100 μg/mL streptomycin, and 2 mM L-glutamine (l11140-050, Invitrogen). Pluripotent cells were maintained on irradiated CF1 MEF feeder layer (catalog number GSC-6001G, GlobalStem). For 2i+ media, 1 μM PD03259010 and 3 μM CHIR99021 (Stemgent) were supplemented into ESC media. For N2/B27 LIF/2i media, 1 μM PD03259010 and 3 μM CHIR99021 were supplemented into a 1:1 mix of DMEM/F12 (11302-033, Life Technologies) and Neurobasal medium (21103-049, Life Technologies) containing N2 and B27 supplements (1:100 dilutions of 17502-048 and 17504- 044, Life Technologies), penicillin/streptomycin, 0.1 mM 2-mercaptoethanol, 2 mM L-glutamine, and LIF. For primed condition media, 10 ng/mL FGF2, 20 ng/mL activin, and 1% KSR were supplemented to the 1:1 DMEM/F12 and Neurobasal medium containing N2 and B27 media, instead of LIF/2i.

Reprogramming Assays

Reprogramming assays were performed as previously described (Onder et al., 2012). For a knockdown experiment, dH1f cells were first infected ~6 days prior to reprogramming with shRNA viruses. For both mouse and human reprogramming, 25,000 fibroblasts were plated per well in 12-well plates and infected overnight with either retroviral or lentiviral factors. Six days later, cells were trypsinized and 25,000 cells were re-plated onto MEF feeder coated 12-well plates. Cells were then fed with ESC medium daily until day 21 when plates were fixed.

Isotope Tracing and Metabolomics Analysis

Isotope tracing and metabolomics studies were performed as described before (Shyh-Chang et al., 2013a). Briefly, 0.5-1 × 10^6 PSCs weaned from MEF feeders were cultured in ESC media (LIF/serum or LIF/2i) containing 25mM [U-^{13}C]-glucose or 2mM [U-^{13}C]-glutamine (Cambridge Isotope Laboratory) with indicated time (Carey et al., 2015). When siRNA was applied, wild-type ESCs were transfected with *lin28a* or *Lin28b* siRNA for 72 hr followed by labeling with [U^{13}C]-glucose with indicated time. Cells or media were subsequently snap-frozen with cold 80% methanol on dry ice, followed by incubation at −80°C from 15 min to overnight. Cells were scraped, collected, and centrifuged at maximum speed for 15 min at 4°C, and the supernatant was evaporated with a speed vacuum at room temperature. Dried sample powder was resuspended with liquid chromatography/mass spectrometry-grade water and applied to a 5500 QTRAP Triple Quadrupole mass spectrometer (AB/SCIEX) coupled to a Prominence HPLC system (Shimadzu) using positive/negative polarity switching via selected reaction monitoring (SRM). Amide hydrophilic interaction chromatography (HILIC; Waters) chromatography was used for metabolite separation. MultiQuant 2.1 software (AB/SCIEX) was used to integrate peak areas from each SRM transition from both unlabeled and ^{13}C-labeled metabolites. (For raw metabolomics data, see Table S1 and Table S2.)

SILAC Analysis for Proteomics

ESCs were cultured in SILAC ESC media made from SILAC Protein Quantification Kit. DMEM media was supplemented with 15% FBS, 1,000 U/mL mLIF (Gemini 400-495), 200 μg/ml penicillin (Corning), 100 μg/mL streptavidin (Corning), 2 mM glutamine (Corning), and 0.1 mM2-mercaptoethanol (Sigma). Knockout *Lin28a*$^{-/-}$, *Lin28b*$^{-/-}$, *or Lin28a*$^{-/-}$*b*$^{-/-}$ ESCs were cultured in light media supplemented with 0.46 mM L-lysine-2HCl, 0.47 mM L-arginine-HCl, and 2 mM proline, whereas wild-type ESCs were cultured in heavy media supplemented with 0.46 mM $^{13}C_6$L-lysine-2HCl, 0.47 mM $^{13}C_6{}^{15}N_4$ L-arginine-HCl, and 2 mM proline. Cells were cultured in heavy and light media for more than 12 days to reach >99% labeling, and 10^7 cells weaned from MEF feeders from heavy and light media, respectively, were mixed, fractionated for cytosol fraction, and applied to mass spectrometry. 500 μg cytosolic proteins was denatured by adding 3.6 M guanidine HCl, reduced with 10 mM

(E) EMSA showing lack of LIN28 binding at *Ndufb10* 3′ RNA oligo for construct expressing cold shock domain only (lacking *GGAG* binding zinc knuckle domains).

(F) EMSA using LIN28 (aa 16–184) and another putative target *Ndufb3* 3′ RNA oligo probe containing *GGAG* and a mutant RNA probe with *GGAG* replaced by *CUCC*.

See also Figure S7.

Tris(2-carboxyethyl)phosphine (TCEP), and alkylated with 20 mM methyl methanethiosulfonate (MMTS). Proteins were diluted with 100 mM ammonium bicarbonate (final guanidine HCl concentration, 1 M) and digested with trypsin (20 μg) overnight at 37°C. Peptides were acidified, and desalted using C18. Detergents from subcellular fractionation were removed by strong cation exchange chromatography. 10 μg peptides was fractionated at high pH (10.0) by reversed-phase chromatography and then by high-pH (10.0) anion exchange chromatography into a total of 21 fractions. Peptide fractions were directly eluted to the final dimension precolumn, resolved with an analytical column, and electrosprayed into the orifice of the mass spectrometer (Orbitrap Fusion, Thermo Fisher Scientific). Data were analyzed as previously described (Parikh et al., 2009). Two biological replicates were analyzed for each phenotype.

ACCESSION NUMBERS

The accession number for the microarray data reported in this paper is GEO: GSE67568.

SUPPLEMENTAL INFORMATION

Supplemental Information includes Supplemental Experimental Procedures, seven figures, and two tables and can be found with this article online at http://dx.doi.org/10.1016/j.stem.2016.05.009.

AUTHOR CONTRIBUTIONS

Conception and design, data analysis, and data interpretation, J.Z., S.R., and G.Q.D.; preparation of the manuscript, J.Z., S.R., M.A.T., J.J.C., and G.Q.D.; reprogramming-related experiments, S.R., Z.W., J.Z., Q.X, S.T., and T.O.; generation and characterization of ESC and iPSC lines, J.Z., S.R., Z.W., G.S., and S.T.; metabolism-related experiments and analysis, J.Z., S.C., S.R., J.M.A., and J.J.C.; microarray, RNA-sequencing, and bioinformatics analysis, J.Z., H.L., C.A.R., S.C., Y.L., M.S., P.C., and J.J.C.; RNA immunoprecipitation (RIP) and chromatin immunoprecipitation sequencing, J.Z., W.X., and Z.W.; proteomics-related experiment and analysis, J.Z., S.B.F., and J.A.M.; in vitro biochemistry experiments, C.Y., J.Z., L.W., and P.S.; and RNA-sequencing and bioinformatics analysis of hiF-T fibroblasts, D.C., C.T., and T.M.

ACKNOWLEDGMENTS

J.J.C. and H.L. were supported by the Howard Hughes Medical Institute, SysCODE (Systems-based Consortium for Organ Design & Engineering), and NIH grant RL1DE019021. H.L. was supported by NIH (grants CA196631-01A1 and 1U54GM114838-01), the Mayo Clinic Foundation, and the Mayo Clinic Center for Individualized Medicine. G.Q.D. was supported by grants from the NIH (R01GM107536, P50GM099117, and U01 HL100001) and by the Ellison Medical Foundation and is an investigator of the Howard Hughes Medical Institute. J.M.A. is supported by NIH grants P01CA120964, S10RR032861, and P30CA006516. We thank Min Yuan and Susanne Breitkopf for help with mass spectrometry experiments; the Marcia Haigis laboratory for Seahorse Analyzer facility; Lewis Cantley and Matthew Vander Heiden for discussion; Michael Chen and the Brigham and Women's Hospital Transgenic Core Facility for help with embryo analysis; The Boston Children's Hospital Molecular Genetics Core Facility for microarray experiments; and Thorsten Schlaeger and the Boston Children's Hospital hESC Core Facility for support with stem cells.

Received: February 5, 2016
Revised: April 11, 2016
Accepted: May 12, 2016
Published: June 16, 2016

REFERENCES

Birsoy, K., Wang, T., Chen, W.W., Freinkman, E., Abu-Remaileh, M., and Sabatini, D.M. (2015). An essential role of the mitochondrial electron transport chain in cell proliferation is to enable aspartate synthesis. Cell *162*, 540–551.

Cacchiarelli, D., Trapnell, C., Ziller, M.J., Soumillon, M., Cesana, M., Karnik, R., Donaghey, J., Smith, Z.D., Ratanasirintrawoot, S., Zhang, X., et al. (2015). Integrative analyses of human reprogramming reveal dynamic nature of induced pluripotency. Cell *162*, 412–424.

Cahan, P., Li, H., Morris, S.A., Lummertz da Rocha, E., Daley, G.Q., and Collins, J.J. (2014). CellNet: network biology applied to stem cell engineering. Cell *158*, 903–915.

Carey, B.W., Finley, L.W.S., Cross, J.R., Allis, C.D., and Thompson, C.B. (2015). Intracellular α-ketoglutarate maintains the pluripotency of embryonic stem cells. Nature *518*, 413–416.

Chan, E.M., Ratanasirintrawoot, S., Park, I.H., Manos, P.D., Loh, Y.H., Huo, H., Miller, J.D., Hartung, O., Rho, J., Ince, T.A., et al. (2009). Live cell imaging distinguishes bona fide human iPS cells from partially reprogrammed cells. Nat. Biotechnol. *27*, 1033–1037.

Chang, T.-C., Zeitels, L.R., Hwang, H.-W., Chivukula, R.R., Wentzel, E.A., Dews, M., Jung, J., Gao, P., Dang, C.V., Beer, M.A., et al. (2009). Lin-28B transactivation is necessary for Myc-mediated let-7 repression and proliferation. Proc. Natl. Acad. Sci. USA *106*, 3384–3389.

Cho, J., Chang, H., Kwon, S.C., Kim, B., Kim, Y., Choe, J., Ha, M., Kim, Y.K., and Kim, V.N. (2012). LIN28A is a suppressor of ER-associated translation in embryonic stem cells. Cell *151*, 765–777.

Faas, L., Warrander, F.C., Maguire, R., Ramsbottom, S.A., Quinn, D., Genever, P., and Isaacs, H.V. (2013). Lin28 proteins are required for germ layer specification in Xenopus. Development *140*, 976–986.

Folmes, C.D., Nelson, T.J., Martinez-Fernandez, A., Arrell, D.K., Lindor, J.Z., Dzeja, P.P., Ikeda, Y., Perez-Terzic, C., and Terzic, A. (2011). Somatic oxidative bioenergetics transitions into pluripotency-dependent glycolysis to facilitate nuclear reprogramming. Cell Metab. *14*, 264–271.

Folmes, C.D., Martinez-Fernandez, A., Faustino, R.S., Yamada, S., Perez-Terzic, C., Nelson, T.J., and Terzic, A. (2013). Nuclear reprogramming with c-Myc potentiates glycolytic capacity of derived induced pluripotent stem cells. J. Cardiovasc. Transl. Res. *6*, 10–21.

Gifford, C.A., Ziller, M.J., Gu, H., Trapnell, C., Donaghey, J., Tsankov, A., Shalek, A.K., Kelley, D.R., Shishkin, A.A., Issner, R., et al. (2013). Transcriptional and epigenetic dynamics during specification of human embryonic stem cells. Cell *153*, 1149–1163.

Hafner, M., Max, K.E.A., Bandaru, P., Morozov, P., Gerstberger, S., Brown, M., Molina, H., and Tuschl, T. (2013). Identification of mRNAs bound and regulated by human LIN28 proteins and molecular requirements for RNA recognition. RNA *19*, 613–626.

Hanna, J., Saha, K., Pando, B., van Zon, J., Lengner, C.J., Creyghton, M.P., van Oudenaarden, A., and Jaenisch, R. (2009). Direct cell reprogramming is a stochastic process amenable to acceleration. Nature *462*, 595–601.

Heo, I., Joo, C., Kim, Y.-K., Ha, M., Yoon, M.-J., Cho, J., Yeom, K.-H., Han, J., and Kim, V.N. (2009). TUT4 in concert with Lin28 suppresses microRNA biogenesis through pre-microRNA uridylation. Cell *138*, 696–708.

Huang, K., Maruyama, T., and Fan, G. (2014). The naive state of human pluripotent stem cells: a synthesis of stem cell and preimplantation embryo transcriptome analyses. Cell Stem Cell *15*, 410–415.

Jin, J., Jing, W., Lei, X.-X., Feng, C., Peng, S., Boris-Lawrie, K., and Huang, Y. (2011). Evidence that Lin28 stimulates translation by recruiting RNA helicase A to polysomes. Nucleic Acids Res. *39*, 3724–3734.

Kumar, R.M., Cahan, P., Shalek, A.K., Satija, R., DaleyKeyser, A.J., Li, H., Zhang, J., Pardee, K., Gennert, D., Trombetta, J.J., et al. (2014). Deconstructing transcriptional heterogeneity in pluripotent stem cells. Nature *516*, 56–61.

Li, N., Zhong, X., Lin, X., Guo, J., Zou, L., Tanyi, J.L., Shao, Z., Liang, S., Wang, L.-P., Hwang, W.-T., et al. (2012). Lin-28 homologue A (LIN28A) promotes cell cycle progression via regulation of cyclin-dependent kinase 2 (CDK2), cyclin D1 (CCND1), and cell division cycle 25 homolog A (CDC25A) expression in cancer. J. Biol. Chem. *287*, 17386–17397.

Lim, J., Ha, M., Chang, H., Kwon, S.C., Simanshu, D.K., Patel, D.J., and Kim, V.N. (2014). Uridylation by TUT4 and TUT7 marks mRNA for degradation. Cell *159*, 1365–1376.

Locasale, J.W. (2013). Serine, glycine and one-carbon units: cancer metabolism in full circle. Nat. Rev. Cancer *13*, 572–583.

Maddocks, O.D.K., Labuschagne, C.F., Adams, P.D., and Vousden, K.H. (2016). Serine metabolism supports the methionine cycle and DNA/RNA methylation through de novo ATP synthesis in cancer cells. Mol. Cell *61*, 210–221.

Madison, B.B., Liu, Q., Zhong, X., Hahn, C.M., Lin, N., Emmett, M.J., Stanger, B.Z., Lee, J.S., and Rustgi, A.K. (2013). LIN28B promotes growth and tumorigenesis of the intestinal epithelium via Let-7. Genes Dev. *27*, 2233–2245.

Marks, H., Kalkan, T., Menafra, R., Denissov, S., Jones, K., Hofemeister, H., Nichols, J., Kranz, A., Stewart, A.F., Smith, A., and Stunnenberg, H.G. (2012). The transcriptional and epigenomic foundations of ground state pluripotency. Cell *149*, 590–604.

Melton, C., Judson, R.L., and Blelloch, R. (2010). Opposing microRNA families regulate self-renewal in mouse embryonic stem cells. Nature *463*, 621–626.

Molenaar, J.J., Domingo-Fernández, R., Ebus, M.E., Lindner, S., Koster, J., Drabek, K., Mestdagh, P., van Sluis, P., Valentijn, L.J., van Nes, J., et al. (2012). LIN28B induces neuroblastoma and enhances MYCN levels via let-7 suppression. Nat. Genet. *44*, 1199–1206.

Nam, Y., Chen, C., Gregory, R.I., Chou, J.J., and Sliz, P. (2011). Molecular basis for interaction of let-7 microRNAs with Lin28. Cell *147*, 1080–1091.

Nguyen, L.H., Robinton, D.A., Seligson, M.T., Wu, L., Li, L., Rakheja, D., Comerford, S.A., Ramezani, S., Sun, X., Parikh, M.S., et al. (2014). Lin28b is sufficient to drive liver cancer and necessary for its maintenance in murine models. Cancer Cell *26*, 248–261.

Onder, T.T., Kara, N., Cherry, A., Sinha, A.U., Zhu, N., Bernt, K.M., Cahan, P., Marcarci, B.O., Unternaehrer, J., Gupta, P.B., et al. (2012). Chromatin-modifying enzymes as modulators of reprogramming. Nature *483*, 598–602.

Parikh, J.R., Askenazi, M., Ficarro, S.B., Cashorali, T., Webber, J.T., Blank, N.C., Zhang, Y., and Marto, J.A. (2009). multiplierz: an extensible API based desktop environment for proteomics data analysis. BMC Bioinformatics *10*, 364.

Park, I.-H., Zhao, R., West, J.A., Yabuuchi, A., Huo, H., Ince, T.A., Lerou, P.H., Lensch, M.W., and Daley, G.Q. (2008). Reprogramming of human somatic cells to pluripotency with defined factors. Nature *451*, 141–146.

Peng, S., Chen, L.-L., Lei, X.-X., Yang, L., Lin, H., Carmichael, G.G., and Huang, Y. (2011). Genome-wide studies reveal that Lin28 enhances the translation of genes important for growth and survival of human embryonic stem cells. Stem Cells *29*, 496–504.

Piskounova, E., Polytarchou, C., Thornton, J.E., LaPierre, R.J., Pothoulakis, C., Hagan, J.P., Iliopoulos, D., and Gregory, R.I. (2011). Lin28A and Lin28B inhibit let-7 microRNA biogenesis by distinct mechanisms. Cell *147*, 1066–1079.

Shinoda, G., Shyh-Chang, N., Soysa, T.Y., Zhu, H., Seligson, M.T., Shah, S.P., Abo-Sido, N., Yabuuchi, A., Hagan, J.P., Gregory, R.I., et al. (2013). Fetal deficiency of lin28 programs life-long aberrations in growth and glucose metabolism. Stem Cells *31*, 1563–1573.

Shiraki, N., Shiraki, Y., Tsuyama, T., Obata, F., Miura, M., Nagae, G., Aburatani, H., Kume, K., Endo, F., and Kume, S. (2014). Methionine metabolism regulates maintenance and differentiation of human pluripotent stem cells. Cell Metab. *19*, 780–794.

Shyh-Chang, N., Locasale, J.W., Lyssiotis, C.A., Zheng, Y., Teo, R.Y., Ratanasirintrawoot, S., Zhang, J., Onder, T., Unternaehrer, J.J., Zhu, H., et al. (2013a). Influence of threonine metabolism on S-adenosylmethionine and histone methylation. Science *339*, 222–226.

Shyh-Chang, N., Zhu, H., Yvanka de Soysa, T., Shinoda, G., Seligson, M.T., Tsanov, K.M., Nguyen, L., Asara, J.M., Cantley, L.C., and Daley, G.Q. (2013b). Lin28 enhances tissue repair by reprogramming cellular metabolism. Cell *155*, 778–792.

Sperber, H., Mathieu, J., Wang, Y., Ferreccio, A., Hesson, J., Xu, Z., Fischer, K.A., Devi, A., Detraux, D., Gu, H., et al. (2015). The metabolome regulates the epigenetic landscape during naive-to-primed human embryonic stem cell transition. Nat. Cell Biol. *17*, 1523–1535.

Sullivan, L.B., Gui, D.Y., Hosios, A.M., Bush, L.N., Freinkman, E., and Vander Heiden, M.G. (2015). Supporting aspartate biosynthesis is an essential function of respiration in proliferating cells. Cell *162*, 552–563.

Takahashi, K., and Yamanaka, S. (2006). Induction of pluripotent stem cells from mouse embryonic and adult fibroblast cultures by defined factors. Cell *126*, 663–676.

Takahashi, K., Tanabe, K., Ohnuki, M., Narita, M., Ichisaka, T., Tomoda, K., and Yamanaka, S. (2007). Induction of pluripotent stem cells from adult human fibroblasts by defined factors. Cell *131*, 861–872.

Takashima, Y., Guo, G., Loos, R., Nichols, J., Ficz, G., Krueger, F., Oxley, D., Santos, F., Clarke, J., Mansfield, W., et al. (2014). Resetting transcription factor control circuitry toward ground-state pluripotency in human. Cell *158*, 1254–1269.

Viswanathan, S.R., and Daley, G.Q. (2010). Lin28: A microRNA regulator with a macro role. Cell *140*, 445–449.

Viswanathan, S.R., Powers, J.T., Einhorn, W., Hoshida, Y., Ng, T.L., Toffanin, S., O'Sullivan, M., Lu, J., Phillips, L.A., Lockhart, V.L., et al. (2009). Lin28 promotes transformation and is associated with advanced human malignancies. Nat. Genet. *41*, 843–848.

Wang, Y., Medvid, R., Melton, C., Jaenisch, R., and Blelloch, R. (2007). DGCR8 is essential for microRNA biogenesis and silencing of embryonic stem cell self-renewal. Nat. Genet. *39*, 380–385.

Wilbert, M.L., Huelga, S.C., Kapeli, K., Stark, T.J., Liang, T.Y., Chen, S.X., Yan, B.Y., Nathanson, J.L., Hutt, K.R., Lovci, M.T., et al. (2012). LIN28 binds messenger RNAs at GGAGA motifs and regulates splicing factor abundance. Mol. Cell *48*, 195–206.

Yan, L., Yang, M., Guo, H., Yang, L., Wu, J., Li, R., Liu, P., Lian, Y., Zheng, X., Yan, J., et al. (2013). Single-cell RNA-Seq profiling of human preimplantation embryos and embryonic stem cells. Nat. Struct. Mol. Biol. *20*, 1131–1139.

Yu, J., Vodyanik, M.A., Smuga-Otto, K., Antosiewicz-Bourget, J., Frane, J.L., Tian, S., Nie, J., Jonsdottir, G.A., Ruotti, V., Stewart, R., et al. (2007). Induced pluripotent stem cell lines derived from human somatic cells. Science *318*, 1917–1920.

Zhang, J., Nuebel, E., Daley, G.Q., Koehler, C.M., and Teitell, M.A. (2012). Metabolic regulation in pluripotent stem cells during reprogramming and self-renewal. Cell Stem Cell *11*, 589–595.

Zhou, W., Choi, M., Margineantu, D., Margaretha, L., Hesson, J., Cavanaugh, C., Blau, C.A., Horwitz, M.S., Hockenbery, D., Ware, C., and Ruohola-Baker, H. (2012). HIF1α induced switch from bivalent to exclusively glycolytic metabolism during ESC-to-EpiSC/hESC transition. EMBO J. *31*, 2103–2116.

Zhu, H., Shyh-Chang, N., Segrè, A.V., Shinoda, G., Shah, S.P., Einhorn, W.S., Takeuchi, A., Engreitz, J.M., Hagan, J.P., Kharas, M.G., et al.; DIAGRAM Consortium; MAGIC Investigators (2011). The Lin28/let-7 axis regulates glucose metabolism. Cell *147*, 81–94.